Crystal Structure of $La_6Mg_4Ta_2W_2O_{24}$ Oxide: A Representative of a Novel $A_{3n}B'_{2n}B''_{2n}O_{12n}$ Homologous Series with $n = 2$

Dmitry D. Khalyavin,* Augusto B. Lopes, Ana M. R. Senos, and Pedro Q. Mantas

Department of Ceramics and Glass Engineering, CICECO, University of Aveiro, 3810-193 Aveiro, Portugal

Received April 20, 2006. Revised Manuscript Received May 29, 2006

The crystal structure of a new A-site deficient $La_6Mg_4Ta_2W_2O_{24}$ perovskite oxide has been solved in the space group $I2/a$ ($a = 7.8711(10)$ Å, $b = 31.9057(10)$ Å, $c = 7.8762(10)$ Å, and $\beta = 90.08(1)°$) from X-ray powder diffraction data. The highest symmetry structural motif which does not involve octahedral tilting is characterized by the *Ibam* space group and represents a sequence of [LaO], [$Mg_{1/2}$-($Ta/W)_{1/2}O_2$], and [$La_{1/2}O$] layers stacked along the *b* axis. The lanthanum ions and the vacancies in the lanthanum poor layers are ordered and form rows along the *c* direction. There are two types of these layers which are shifted between each other in a half period along the *a* axis. The alternation of the lanthanum poor layers with the lanthanum rich ones, along with the rock salt type cation ordering between Mg^{2+} and Ta^{5+}/W^{6+}, results in a $2a_p \times 8a_p \times 2a_p$ type superstructure. An antiphase octahedral tilting around the *b* axis reduces the symmetry from orthorhombic *Ibam* to monoclinic $I2/a$. The number of equivalent [$La_{1/2}O$] layers, *n*, contained in a unit cell of the parent untilted crystal structure allows a new homologous series, $A_{3n}B'_{2n}B''_{2n}O_{12n}$, with the common *Ibam* space group and $2a_p \times 4na_p \times 2a_p$ type superstructure to be identified. The $La_6Mg_4Ta_2W_2O_{24}$ oxide is a representative with $n = 2$.

Introduction

A-site deficient perovskite-like oxides are of great interest both as components for dielectric resonators in microwave applications[1,2] and as ion-conducting solid electrolytes for electrochemical devices.[3,4] A known example with partially ordered A-site vacancies in the (001) planes is $La_{2/3}TiO_3$. Some dielectric materials with good electrical characteristics[5,6] and lithium conductors with high ionic conductivity[7−9] have been developed on the basis of this compound. The high temperature ($T > 640$ K) crystal structure of $La_{2/3}TiO_3$ can be represented by a sequence of the layers [LaO]−[TiO_2]−[$La_{1/3}O$]−[TiO_2], stacked along the *c* axis of the *P*4/*mmm* space group.[10,11] The alternation of the fully and partially occupied (001) planes containing lanthanum forms a tetragonal superstructure of the $a_p \times a_p \times 2a_p$ type (a_p is the parameter of the primitive perovskite unit cell). The cation vacancies in the lanthanum poor layers, [$La_{1/3}O$], are distributed randomly. Below 640 K, the crystal structure has the orthorhombic *Cmmm* symmetry and involves antiphase rotations of the TiO_6 octahedra around the axis perpendicular to the direction of the cation ordering.

The crystal structure of $La_4Mg_3W_3O_{18}$ ($La_{2/3}Mg_{1/2}W_{1/2}O_3$) is closely related to the structure of $La_{2/3}TiO_3$.[12] Above 700 K, this compound is characterized by the orthorhombic *Ibam* symmetry with $2a_p \times 4a_p \times 2a_p$ type superstructure and presents a sequence of [LaO]−[$Mg_{1/2}W_{1/2}O_2$]−[$La_{1/3}O$]′−[$Mg_{1/2}W_{1/2}O_2$]−[LaO]−[$Mg_{1/2}W_{1/2}O_2$]−[$La_{1/3}O$]″−[$Mg_{1/2}$-$W_{1/2}O_2$] layers stacked along the *b* axis. The lanthanum ions and the vacancies in the lanthanum poor layers, [$La_{1/3}O$]′ and [$La_{1/3}O$]″, are ordered and form rows along the *c* axis. A half-period shift along the *a* direction between these layers leads to a quadrupling of the primitive perovskite unit cell in the *b* direction. Below 700 K, the symmetry is lowered to monoclinic *C*2/*m* as a result of an antiphase rotation of the octahedra around the axis parallel to the lanthanum formed rows.

However, as already pointed out in ref 12, $La_4Mg_3W_3O_{18}$ is not stoichiometric in respect to the structural type described above. The 4*a* position in the *Ibam* space group (lanthanum position within the [$La_{1/3}O$]′ and [$La_{1/3}O$]″ layers) is only 2/3 occupied, and the full occupation of the position would require the chemical formula to be $La_3Mg_2W^{5+}W^{6+}O_{12}$. Thus, if half of the +6 B-site cations, actually W, could be replaced by +5 cations, there is the possibility to obtain a crystal

* To whom correspondence should be addressed. E-mail: dkhalyavin@cv.ua.pt.

(1) Lee, H. J.; Son, J. O.; Oh, S. H.; Chom, Y. K.; Nahm, S. *Jpn. J. Appl. Phys.* **2004**, *43*, 7587−7591.
(2) Skapin, S. D.; Suvorov, D. *Mater. Sci. Forum.* **2003**, *413*, 115−120.
(3) Stramare, S.; Thangadurai, V.; Weppner, W. *Chem. Mater*. **2003**, *15*, 3974−3990.
(4) Ruiz, A. I.; Lopez, M. L.; Pico, C.; Santrich-Badal, A.; Veiga, M. L. *J. Solid State Chem.* **2003**, *173*, 130−136.
(5) Vanderah, T. A.; Miller, V. L.; Levin, I.; Bell, S. M.; Negas, T. *J. Solid State Chem.* **2004**, *177*, 2023−2038.
(6) Salak, A. N.; Khalyavin, D. D.; Mantas, P. Q.; Senos, A. M. R.; Ferreira, V. M. *J. Appl. Phys.* **2005**, *98*, 034101.
(7) Inaguma, Y.; Chen, L. Q.; Itoh, M.; Nakamura, T.; Uchida, T.; Ikuta, H.; Wakihara, M. *Solid State Commun.* **1993**, *86*, 689−693.
(8) Ibarra, J.; Varez, A.; Leon, C.; Santamaria, J.; Torres-Martinez L. M.; Sanz, J. *Solid State Ionics* **2000**, *134*, 218−228.
(9) Morata-Orrantia, A.; Garcia-Martin, S.; Alario-Franco, M. A. *Chem. Mater.* **2003**, *15*, 3991−3995.
(10) Howard, C. J.; Zhang, Z. *J. Phys.: Condens. Matter* **2003**, *15*, 4543−4553.
(11) Yashima, M.; Mori, M.; Kamiyama, T.; Oikawa, K.; Hoshikawa, A.; Torii, S.; Saitoh, K.; Tsuda, K. *Chem. Phys. Lett*. **2003**, *375*, 240−246.
(12) Khalyavin, D. D.; Senos, A. M. R.; Mantas, P. Q. *J. Phys.: Condens. Matter* **2005**, *17*, 2585−2595.

10.1021/cm060916q CCC: $33.50
Published on Web 07/07/2006

structure with all the 4*a* position occupied by an atom. Upon trying to do this by substituting half of the W^{6+} by Ta^{5+}, $La_3Mg_2Ta^{5+}W^{6+}O_{12}$, we arrived at another structural type for the compound, although related to $La_4Mg_3W_3O_{18}$, which we report here. The identification of a new homologous series of the type $A_{3n}B'_{2n}B''_{2n}O_{12n}$, due to the relation between the crystal structures of the two compounds, is discussed.

Experimental Section

To prepare the $La_6Mg_4Ta_2W_2O_{24}$ oxide, powders of La_2O_3 (99.5%, Merck), MgO (98%, Fluka), Ta_2O_5 (99.9%, Riedel−de Haën), and WO_3 (99.9%, Fluka) were weighed according to the stoichiometry of the composition and mixed for 4 h, in a polyethylene container with ethanol and zirconia balls, in a planetary mill. The slurries were dried in an oven at 120 °C, and the dried powders were de-agglomerated. The powders were then calcined at 1200 °C for 4 h. After calcination, the materials were de-agglomerated again. Finally, pellets with 10 mm diameter and 5−6 mm height were obtained by uniaxial pressing in a steel die under 60 MPa, followed by an isostatic pressing at 200 MPa. The pellets were sintered in air for 6 h at 1500 °C. The heating and cooling rates were 100 °C/h. Weight losses during the sintering did not exceed 1.5%. The microstructure and cation composition of the sintered specimens were characterized by scanning electron microscopy (SEM) and electron-dispersive spectrometry (EDS) analysis, respectively, using a Hitachi S-4100 microscope equipped with a Rontec spectrometer.

To obtain powders for X-ray powder diffraction (XRD) experiments the sintered pellets were crushed in an agate mortar. The room-temperature XRD data were collected using a Rigaku D/MAX-B diffractometer (Cu Kα radiation; tube power 40 kV, 30 mA; 2θ range 0−120°, step 0.02°, 20 s/step; graphite monochromator; receiving slit 0.15 mm). The high-temperature XRD experiments were carried out on a Philips X′Pert MPD diffractometer (Cu Kα radiation; tube power 40 kV, 30 mA; graphite monochromator, step 0.01°, 20 s/step; receiving slit 0.15 mm). For the temperature evolution only selected reflections were examined. The obtained data were refined by the Rietveld method using the Fullprof program[13] and assuming a pseudo-Voigt profile shape function. The background was described by interpolation between selected points.

For electron diffraction, samples were mounted on a glass slide using a thermally sensitive resin and ground to approximately 30 μm. A Cu support ring was then glued to the samples using an epoxy resin. The samples were removed from the slide, and excess ceramic was chipped away from around the support ring. The samples were then ion beam milled until perforation using a BALTEC Ion Mill (RES 100), at an angle of 20°, an accelerating voltage of 6 kV, and a total gun current of 2.3 mA. The final step of preparation was made using an 8° angle. Samples were examined using a Hitachi H9000-NA transmission electron microscope, operating at an accelerating voltage of 300 kV.

Results and Discussion

The analysis of the XRD spectrum of $La_6Mg_4Ta_2W_2O_{24}$ revealed that this composition crystallizes into a structure different from the one reported for $La_4Mg_3W_3O_{18}$.[12] The large number of reflections with intermediate and small intensity (Figure 1) points to a complex cation distribution and makes the indexation procedure difficult. They could also come

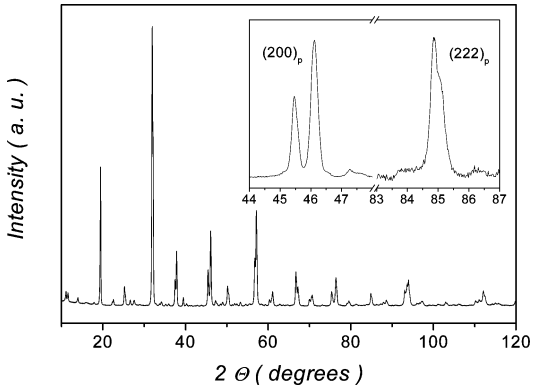

Figure 1. XRD pattern of $La_6Mg_4Ta_2W_2O_{24}$. The inset shows the $(200)_p$ and $(222)_p$ normalized fundamental multiplets.

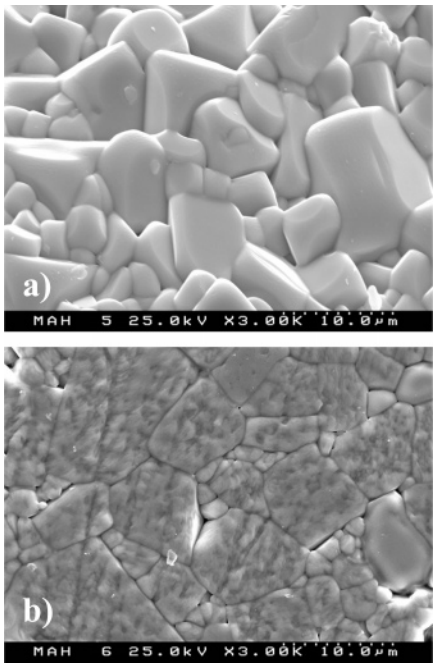

Figure 2. SEM observation of the microstructure of $La_6Mg_4Ta_2W_2O_{24}$ sintered at 1500 °C: (a) fractured surface and (b) polished and thermally etched surface.

from the presence of a crystalline secondary phase, but SEM observations (Figure 2) revealed a dense and homogeneous material, without any other phases. The chemical composition determined by EDS is the same as the starting one. This points to the case where all the reflections belong to the same phase. The microstructure of the sample sintered at 1500 °C is also different from that observed in $La_4Mg_3W_3O_{18}$. In the present case there is not a strong anisotropy in the shape of the grains, a phenomenon clearly observed in $La_4Mg_3W_3O_{18}$ sintered at temperatures higher than 1400 °C.

A set of reflections corresponding to the fundamental multiplets of the aristotype perovskite structure can be distinguished in the XRD spectrum. The splitting of some of these $(hkl)_p$[14] reflections into doublets for $h = k \neq l$ and the nonsplitting of the reflections for $h = k = l$ (Figure 1, inset) are consistent with a tetragonal metric of the primitive perovskite unit cell, in the framework of the instrument resolution. To pursue the analysis of the crystal structure, we choose the setting where $b_p > a_p \approx c_p$. The presence of

(13) Rodriguez-Carvajal, J. *Physica B* **1993**, *192*, 55−69.

(14) The subscript p indicates a primitive perovskite unit cell indexation.

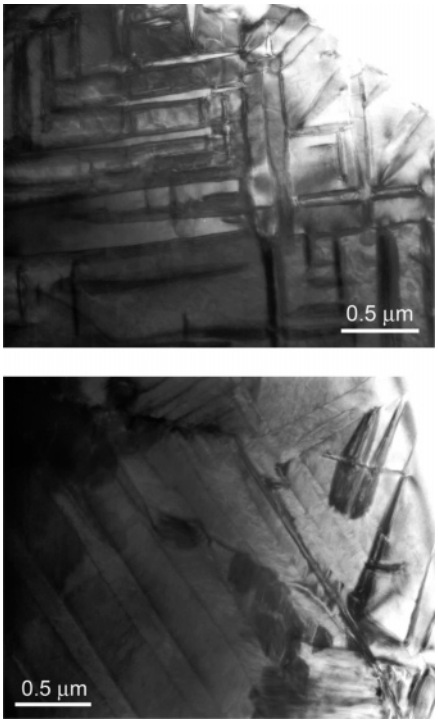

Figure 3. TEM image illustrating the twinned structure of the grains.

strong superstructure reflections of the $^1/_2(hkl;\ h,\ k,\ l = 2n + 1)_p$ and $^1/_2(hkl;\ h,\ l = 2n,\ k = 2n + 1)_p$ types provides evidence for the ionic ordering between Mg^{2+} and Ta^{5+}/W^{6+} into a NaCl lattice type and the alternation of the fully and partially occupied lanthanum containing planes along the *b* direction, respectively. The rock-salt type of the ionic ordering in the B-site position, in combination with the layer type ordering in the A-site position, results in the *P*4/*nmm* space group with a $\sqrt{2}a_p \times \sqrt{2}a_p \times 2a_p$ unit cell. However, there is a number of reflections which cannot be indexed in this unit cell, and it is necessary to enlarge the unit cell dimension or to include an incommensurate sublattice to successfully index them.

To determine the cell parameters, we used the electron diffraction experiments performed on numerous grains. Despite the complex microstructure of the grains (Figure 3) and frequent observation of 90° oriented twins, the reconstruction of the reciprocal space could be performed. Figure 4 shows the [100], [010], and [001] zone axis electron diffraction patterns. Two sets of reflections can be distinguished through their relative intensity: the stronger one, which is related to a $a_p \times 2b_p \times c_p$ subcell, and the weaker one, which leads to the $2a_p \times 8b_p \times c_p$ orthorhombic unit cell.

Taking into account the NaCl type ordering in the B-site position doubling the primitive perovskite unit cell in all the three directions, a $2a_p \times 8b_p \times 2c_p$ type cell was successfully used in the indexation procedure of the XRD pattern. The $(h + k + l = 2n)_s$[15] reflection condition indicates a body-centered Bravais lattice. Although the primitive unit cell is close to a tetragonal metric, the $2a_p \times 8a_p \times a_p$ type superstructure observed in the electron diffraction points to

(15) The subscript s indicates that the *h*, *k*, and *l* indexes are related to the unit cell with $2a_p \times 8b_p \times 2c_p$ dimension.

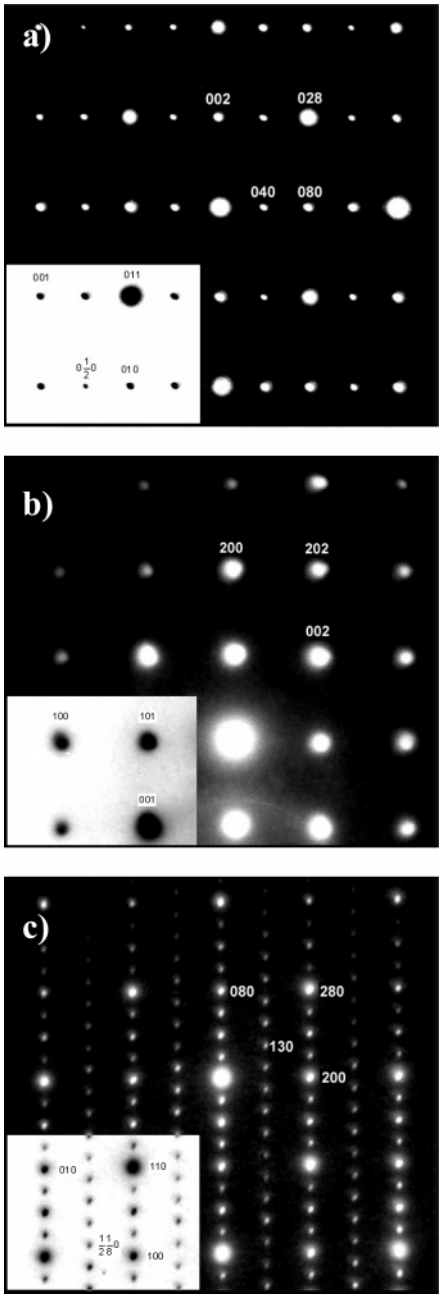

Figure 4. In parts a−c, the electron diffraction patterns of the [100], [010], and [001] axes are shown, respectively, demonstrating the corresponding reflection conditions of $(0kl;\ k,\ l = 2n)_s$, $(h0l;\ h,\ l = 2n)_s$, and $(hk0;\ h + k = 2n)_s$. The insets show primitive unit cell indexation.

an orthorhombic symmetry of the crystal structure. The reflection conditions $(0kl;\ k,\ l = 2n)_s$, $(h0l;\ h,\ l = 2n)_s$, and $(hk0;\ h + k = 2n)_s$, deduced from the electron diffraction, are consistent with the *Ibam* space group, which also characterizes the high temperature untilted phase of $La_4Mg_3W_3O_{18}$.[12] In the [001] electron diffraction pattern there are also reflections of the $(h,\ k + {}^1/_4,\ 0)_p$ type, which are absent in the XRD spectrum. These reflections are probably caused by dynamical effects, since they can be explained by the simple superposition of $(h + {}^1/_2,\ k + {}^1/_8,\ 0)_p + (h + {}^1/_2,\ k + {}^1/_8,\ 0)_p \rightarrow (h,\ k + {}^1/_4,\ 0)_p$.

We can conclude at this stage that $La_6Mg_4Ta_2W_2O_{24}$ is characterized by the *Ibam* space group with a $2a_p \times 8a_p \times 2a_p$ supercell. A possible representation of such crystal structure is shown in Figure 5a. For a comparison, the high

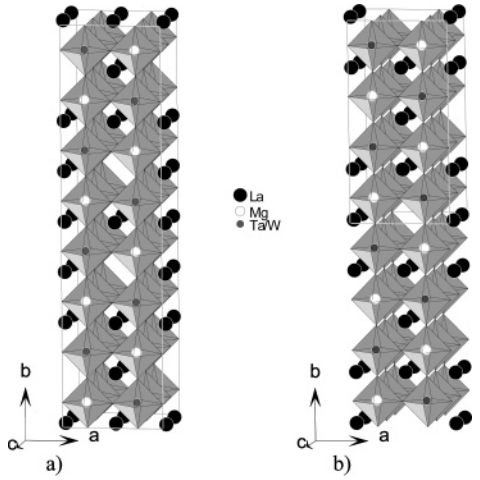

Figure 5. Schematic representation of the crystal structure (without octahedral tilting) of $La_6Mg_4Ta_2W_2O_{24}$ (a) and $La_4Mg_3W_3O_{18}$ (b).

temperature ($T > 700$ K) crystal structure of $La_4Mg_3W_3O_{18}$ is also presented (Figure 5b). In both cases there is an alternation between the lanthanum rich, [LaO], and the lanthanum poor, $[La_{1/2}O]'/[La_{1/2}O]''$, layers. The lanthanum ions and vacancies are ordered in the lanthanum poor layers, forming rows along the *c* direction. The half-period shift along the *a* direction, giving origin to the nonequivalent $[La_{1/2}O]'$ and $[La_{1/2}O]''$ layers, happens differently in the two cases: in the case of $La_4Mg_3W_3O_{18}$, the sequence is $[La_{1/2}O]'\cdots[La_{1/2}O]''\cdots[La_{1/2}O]'\cdots[La_{1/2}O]''$, whereas in the case of $La_6Mg_4Ta_2W_2O_{24}$ the sequence is $[La_{1/2}O]'\cdots[La_{1/2}O]'\cdots[La_{1/2}O]''\cdots[La_{1/2}O]''$. The refinement of the XRD spectrum confirmed the accuracy of the proposed model, and a convergence was reached in the *Ibam* space group with quite good agreement factors: $R_p = 14.5\%$ and $R_{wp} = 15.4\%$.

A comparison of the structures shown in Figure 5a,b leads to the conclusion that, depending on the number of paired $[La_{1/2}O]'$ and $[La_{1/2}O]''$ layers, *n*, contained in the unit cell, different structural types with a $2a_p \times 4na_p \times 2a_p$ supercell and *Ibam* space group can be obtained. In other words, both these structural types can be combined into homologous series where $La_4Mg_3W_3O_{18}$ is a representative of $n = 1$ and $La_6Mg_4Ta_2W_2O_{24}$ is a representative of $n = 2$. Each member of the series can be obtained by repeating *n* times the following structural blocks: $[AO]-[B'_{1/2}B''_{1/2}O_2]-[A_{1/2}O]'-[B'_{1/2}B''_{1/2}O_2]-[AO]-[B'_{1/2}B''_{1/2}O_2]-[A_{1/2}O]''-[B'_{1/2}B''_{1/2}O_2] \equiv A_3B'_2B''_2O_{12}$. Therefore, the chemical formula for any member can be written as $A_{3n}B'_{2n}B''_{2n}O_{12n}$. When this nomenclature is used, the chemical formula of $La_4Mg_3W_3O_{18}$ should be rewritten as $La_{8/3}Mg_2W_2O_{12}$ to emphasize the fact that the composition belongs to the $n = 1$ family.

By analogy with $La_4Mg_3W_3O_{18}$[12] and $La_{2/3}TiO_3$,[10,11] one can suppose that the symmetry of $La_6Mg_4Ta_2W_2O_{24}$ at room temperature is lower than the one given by the *Ibam* space group as a result of oxygen displacements (octahedral tilting). In ref 12 we presented a symmetry analysis of the crystal structures which can be derived from the *Ibam* one as a result of an octahedral rotation around one of the crystallographic directions. Before the discussion of a possible tilted system, we point out that, in the untilted crystal structure shown in Figure 5a, a very close to tetragonal metric of the primitive unit cell is expected (like in the case of the high-temperature phase of $La_4Mg_3W_3O_{18}$). The tetragonal metric is caused by the fact that along the *a* and *c* directions the alternation of the planes equivalently occupied by lanthanum ions takes place.

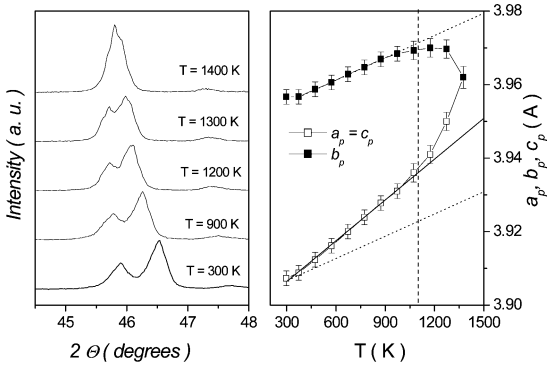

Figure 6. Temperature evolution of the $(200)_p$ fundamental multiplet (left panel) and the primitive perovskite translations in the tetragonal approximation (right panel). The vertical dashed line corresponds to the temperature at which the nonlinear variation of the parameters starts. The dotted and solid lines of the slopes are guides to better visualize the anisotropy of the thermal expansion of the b_p and $a_p \approx c_p$ parameters.

Any type of octahedral tilting (in-phase or antiphase) around the *a* or *c* axis must lead to an orthorhombic metric of the primitive perovskite unit cell, which is not consistent with the observations, because within the instrument resolution, the metric of the primitive unit cell is tetragonal. In the case of a rotation of the octahedra around the *b* axis, a tetragonal metric will be kept; however, the value of the tetragonal distortions will depend on the rotation angle and, consequently, on the temperature. In other words, if either an $a^0b^+c^0$ or an $a^0b^-c^0$ tilted configuration is being realized in $La_6Mg_4Ta_2W_2O_{24}$, the thermal expansion of the a_p and c_p parameters will be much higher than that of the b_p one. To check this possibility, high-temperature XRD studies have been performed. The temperature evolution of the $(200)_p$ fundamental multiplet was examined (Figure 6, left panel). A behavior of the parameters of the primitive perovskite unit cell in the tetragonal approximation ($a_p \approx c_p \neq b_p$) is shown in the right panel of Figure 6. The strong anisotropy of the thermal expansion of the b_p and $a_p \approx c_p$ parameters can be clearly seen. Below $T \sim 1100$ K, both parameters change almost linearly, with a much higher slope in the case of $a_p \approx c_p(T)$. This observation is consistent with the assumption that octahedral rotation around the *b* axis takes place. Above $T = 1100$ K, the behavior of both parameters is nonlinear, and they merge together when the temperature is $T \sim 1400$ K. This behavior can be assigned to an order−disorder transition between lanthanum ions and vacancies in the A-site perovskite position. Examination of the fundamental multiplets allowed us to conclude that this transition is accompanied by a change of the tilted configuration too. Detailed structural investigations of the high-temperature phase transformations in $La_6Mg_4Ta_2W_2O_{24}$ are outside of the matter of the present work and will be reported in a separate paper. But it should be noted here that the order−disorder transition can explain the difference in the microstructures between $La_4Mg_3W_3O_{18}$ and $La_6Mg_4Ta_2W_2O_{24}$. In the last case, the grain growth occurs in the temperature range where the disordered phase is observed which does not induce a pronounced crystallographic anisotropy effect.

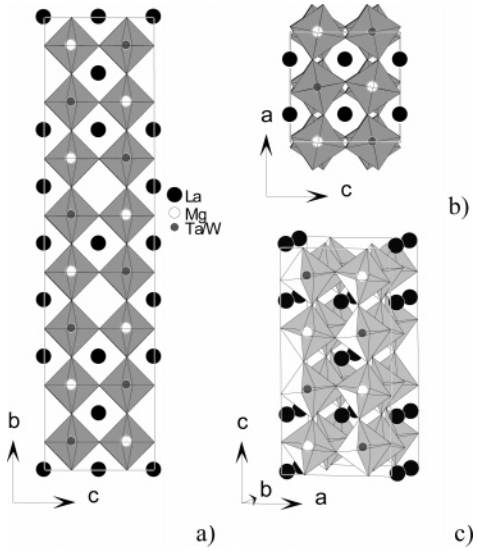

Figure 7. Schematic representation of the crystal structure with octahedral tilting for $La_6Mg_4Ta_2W_2O_{24}$ (a, b) and for $La_4Mg_3W_3O_{18}$ (c).

Thus, taking into account the high-temperature XRD data and using the result of the group-theoretical analysis,[12] the symmetry of $La_6Mg_4Ta_2W_2O_{24}$ at room temperature can be either orthorhombic $I222$ ($a^0b^+c^0$) or monoclinic $C2/c$ ($a^0b^-c^0$). For the first case, the presence of the $^1/_2(hkl$; h, $l = 2n + 1$, $k = 2n)_p$ superstructure reflections from the in-phase octahedral tilting is expected. They were not observed, neither in the room-temperature XRD spectrum nor in the electron diffraction patterns, and, therefore, the monoclinic $C2/c$ space group is the most appropriate one for the description of the room-temperature crystal structure of $La_6Mg_4Ta_2W_2O_{24}$. It should be noted that the direct conclusion about the monoclinic symmetry based only on the room-temperature XRD spectrum and on the electron diffraction patterns is strongly complicated by the overlapping of the superstructure reflections coming from the antiphase octahedral tilting and from the rock-salt type ionic ordering in the B-site position, with much higher structural factors.

The lattice vectors of the $C2/c$ space group ($\vec{a}_m$, $\vec{b}_m$, $\vec{c}_m$) in terms of the parent *Ibam* ones ($\vec{a}_o$, $\vec{b}_o$, $\vec{c}_o$) can be expressed as $\vec{a}_m = \vec{a}_o - \vec{c}_o$, $\vec{b}_m = \vec{b}_o$, and $\vec{c}_m = \vec{c}_o$, which gives the monoclinic angle, β, $\sim 135°$. To visualize the tilted crystal structure (Figure 7) and to refine the XRD spectrum (Figure 8), we used the nonstandard setting (monoclinic cell choice 3) which results in a near orthogonal unit cell $\vec{a}_m = \vec{c}_o$, $\vec{b}_m = \vec{b}_o$, and $\vec{c}_m = \vec{a}_o$ and a $I2/a$ symbol for the space group. Initial atomic coordinates were generated using the ISOTROPY software[16] from the parent (untilted) structure and the Γ_4^+ irreducible representation of the *Ibam* space group. The positions in the parent structure were calculated from 1*a*, 1*b*, and 3*d* Wyckoff positions in the simple cubic perovskite structure and $Z_4(k = {}^1/_8, {}^1/_2, 0) \oplus R_1^+(k = {}^1/_2, {}^1/_2, {}^1/_2)$ representation of the $Pm\bar{3}m$ space group.

In the beginning the refinement was carried out without any constraints, and a convergence was reached with the agreement factors $R_p = 12.7\%$ and $R_{wp} = 13.7\%$. However,

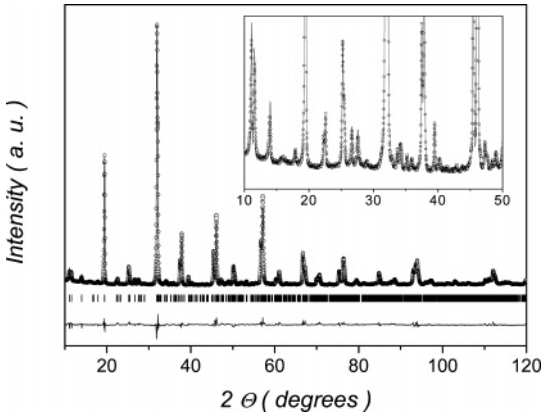

Figure 8. Observed (circles), calculated (continuous curve), and difference (solid line below the spectrum) room-temperature XRD patterns of $La_6Mg_4Ta_2W_2O_{24}$. The vertical bars correspond to the calculated peak positions. The inset shows an expanded view of the 10−50° 2θ range.

the examination of the bond distances revealed very poor local crystal chemistry with improbably distorted octahedra. It is not surprising because the proposed structural model contains 12 oxygen ions in general positions. Therefore, to obtain a good first approximation to the structure, a set of constraints for the refinement of the oxygen coordinates was applied. They were deduced on the assumption of rigid octahedra tilted in the $a^0b^-c^0$ configuration. This approach is similar to that used by Ting et al.[17] for nominally independent atomic displacements in the $A_3CoNb_2O_9$ (A = Ca, Sr, Ba) ordered pervskites involving an octahedral tilting. The first parameter, taken with an appropriate sign, varied the *y* component of the oxygen atoms lying on the *b* axis (O9−O12). The variation of this component is dictated by the difference in the size of the MgO_6 and the Ta/WO_6 octahedrons. The same reason implies a variation of the *x* and *z* components for O5−O8 and O1−O4, respectively. We used the same parameter for the *x* and the *z* components because of the pseudo-tetragonal metric of the unit cell suggesting that in a first approximation the octahedra are isotropic in the *a* and *c* directions. The third parameter was responsible for the octahedral rotation around the *b* axis. It varied the *x* and *z* components of the O1−O4 and O5−O8 oxygen atoms, respectively. After refinement of these 20 constrained oxygen coordinates, the agreement factors were reduced down to $R_p = 12.8\%$ and $R_{wp} = 13.9\%$ (before varying the oxygen positions $R_p = 14.5\%$ and $R_{wp} = 15.4\%$). The main improvement came from the variation of the third parameter, which confirms the correct choice of the tilt system. The variation of the other oxygen coordinates is required by neither the difference in the size of the B-site cations nor by the $a^0b^-c^0$ configuration. However, some of the oxygen ions, namely, O1, O2 and O10, O12, have a nonsymmetrical surrounding of the vacancies and lanthanum ions in their first coordination sphere. This asymmetry can originate gradients of the local electrical fields and, consequently, additional shifts of these oxygen ions. From symmetry consideration, it can be concluded that the directions of the most probable displacements of the O1, O2 and O10, O12 ions are along the *b* and *c* axes, respectively. Therefore,

(16) Stokes, H. T.; Hatch, D. M. *ISOTROPY*; Brigham Young University: Provo, UT, 2002 (http://stokes.byu.edu/isotropy.html).

(17) Ting, V.; Liu, Y.; Noren, L.; Withers, R. L.; Goossens, D. J.; James, M.; Ferraris, C. *J. Solid State Chem.* **2004**, *177*, 4428−4442.

Table 1. Atomic Coordinates and Isotropic Thermal Parameters (B_{iso}) for $La_6Mg_4Ta_2W_2O_{24}$ at Room Temperature[a]

atom	position	occupation	*x*	*y*	*z*	B_{iso} (Å^2)
La1	4e	0.920(3)	0.25	0.2538(2)	0	0.23(3)
La2	4e	0.920(3)	0.25	−0.2536(3)	0	0.23(3)
La3	4e	0.920(3)	0.25	0.0002(6)	0	0.23(3)
La4	4*e*	0.855(3)	0.25	−0.3754(4)	0	0.23(3)
La5	4e	0.855(3)	0.25	0.3765(6)	0	0.23(3)
La6	4e	0.920(3)	0.25	0.4999(6)	0	0.23(3)
La7	4e	0.225(3)	0.25	0.1251(3)	0	0.23(3)
La8	4e	0.225(3)	0.75	0.1244(6)	0	0.23(3)
Mg1	8f	1	0.0004(12)	−0.1865(4)	−0.2461(30)	0.61(19)
Mg2	8f	1	0.0004(12)	0.0635(4)	−0.2461(30)	0.61(19)
Ta/W1	8f	1	0.0001(2)	−0.0645(1)	−0.2419(4)	0.08(3)
Ta/W2	8f	1	0.0001(2)	0.1855(1)	−0.2419(4)	0.08(3)
O1	8f	1	−0.0481(13)	−0.1910(15)	0.0034(7)	1.04(18)
O2	8f	1	0.0481(13)	−0.0564(13)	−0.0034(7)	1.04(18)
O3	8f	1	−0.0481(13)	0.3125(−)[b]	0.0034(7)	1.04(18)
O4	8f	1	0.0481(13)	0.4375(−)[b]	−0.0034(7)	1.04(18)
O5	8f	1	0.2466(10)	0.3125(−)[b]	0.2019(13)	1.04(18)
O6	8f	1	0.2534(10)	−0.3125(−)[b]	0.2981(13)	1.04(18)
O7	8f	1	0.2534(10)	0.4375(−)[b]	0.2981(13)	1.04(18)
O8	8f	1	0.2466(10)	−0.4375(−)[b]	0.2019(13)	1.04(18)
O9	8f	1	0.0000(−)[b]	−0.2515(25)	−0.2500(−)[b]	1.04(18)
O10	8f	1	0.0000(−)[b]	−0.1235(25)	−0.256(11)	1.04(18)
O11	8f	1	0.0000(−)[b]	−0.0015(25)	−0.2500(−)[b]	1.04(18)
O12	8f	1	0.0000(−)[b]	0.1265(25)	−0.256(11)	1.04(18)

[a] Space group *I*2/*a*; cell parameters $a = 7.8711(10)$ Å, $b = 31.9057(10)$ Å, $c = 7.8762(10)$ Å, $\beta = 90.08(1)°$, $V = 1977.97(20)$ Å^3; and $Z = 16$; calculated density of 6.884 g/cm^3. Reliability factors: conventional Rietveld *R* factors, $R_p = 12.7\%$ and $R_{wp} = 13.8\%$; not corrected for background, $R_p = 6.78\%$ and $R_{wp} = 8.93\%$. [b] Some of the oxygen coordinates were fixed during the refinement (see the text for the explanation). The isotropic thermal parameters were constrained to be equal for the same atom types.

four additional variation parameters were introduced. The refinement with the 24 constrained oxygen coordinates gave $R_p = 12.7\%$ and $R_{wp} = 13.8\%$. In this stage the refinement was stopped because the agreement factors were very close to those obtained in the unconstrained refinement and there were no obvious reasons for additional oxygen displacements, which can be detected by XRD. The crystallographic parameters obtained in this refinement are listed in Table 1, and a schematic representation of the crystal structure is shown in Figure 7. The observed and calculated XRD patterns as well as the difference between them are displayed in Figure 8. Additional structural information (bond distances, angles, and valence sums) can be found in Supporting Information.

The ionic ordering in the $[Mg_{1/2}(Ta/W)_{1/2}O_2]$ blocks plays an important role in the formation of the lanthanum vacancy rows. A smaller electrostatic repulsion between neighbor cations in the ordered state allows them to be significantly displaced toward the vacancy to compensate for the deficiency in positive charge[18] (Figure 9). These displacements are the origin for local distortions, which have opposite sign in neighbor (010) planes (in Figure 9, the local distortions are represented by lozenges). The half-period shift between the $[La_{1/2}O]'$ and $[La_{1/2}O]''$ layers avoids a cooperative character of these distortions within a whole (010) plane. The local distortions arise because of a difference in the size and charge of the B-site cations and, consequently, because of their nonequal displacement amplitudes. The stronger the difference between the B′ and B″ cations, the larger the local distortions. In the case of $La_4Mg_3W_3O_{18}$, the difference in

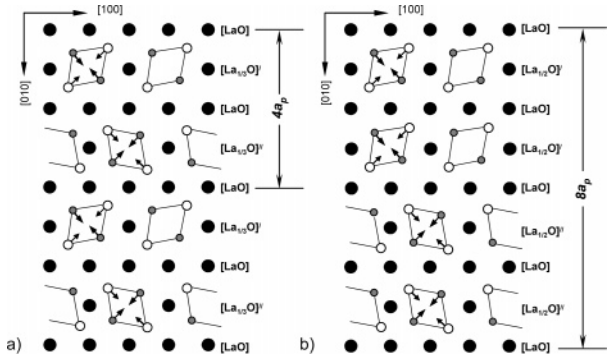

Figure 9. Schematic representation of the magnesium/(tantalum, tungsten) cation displacements in the (010) planes in the cases of $2a_p \times 4a_p \times a_p$ ($La_4Mg_3W_3O_{18}$; a) and $2a_p \times 8a_p \times a_p$ ($La_6Mg_4Ta_2W_2O_{24}$; b) superstructures. The local distortions are represented by lozenges.

the charge between B-site cations is 4 and strong local distortions result in the appearance of the half-period shift between neighbor lanthanum poor layers. The substitution of W^{6+} by Ta^{5+} decreases the charge difference between the B-site cations (to 3.5 in $La_6Mg_4Ta_2W_2O_{24}$) and leads to a smaller amount of vacancies in the lanthanum poor layers. Both effects reduce the local distortions and increase the size of the "domain (number of equivalent lanthanum poor layers)" with the same sign of the local distortions. Thus, the strategy to stabilize the members of the $A_{3n}B'_{2n}B''_{2n}O_{12n}$ homologous series with $n > 1$ is both to reduce the difference between B′ and B″ cations and to decrease the amount of vacancies in the lanthanum poor layers. On the other hand, the concentration of the vacancies should be large enough to keep the layer character of the crystal structure.

Conclusions

A new A-site deficient perovskite $La_6Mg_4Ta_2W_2O_{24}$ has been synthesized by the conventional solid-state reaction

(18) Probably the important factor stabilizing the layer type structure is also the second-order Jahn−Teller nature of octahedrally coordinated W^{6+} and Ta^{5+} ions which favors the significant displacements of these ions. Knapp, M. C.; Woodward, P. M. *J. Solid State Chem.* **2006**, *179*, 1065−1074.

method. The crystal structure at room temperature involves an A-site vacancy ordering and an oxygen octahedral tilting, which results in the monoclinic *I*2/*a* symmetry with the parameters of the unit cell being $a = 7.8711(10)$ Å, $b = 31.9057(10)$ Å, $c = 7.8762(10)$ Å, and $\beta = 90.08(1)°$. The untilted crystal structure, keeping the oxygen ions in their highly symmetric positions, is characterized by the orthorhombic *Ibam* symmetry and can be represented as a sequence of the [LaO], $[Mg_{1/2}(TaW)_{1/2}O_2]$, and $[La_{1/2}O]$ layers stacked along the *b* axis. The lanthanum ions and the vacancies in the lanthanum poor layers are ordered and form rows along the *c* axis. There are two types of the lanthanum poor layers, $[La_{1/2}O]'$ and $[La_{1/2}O]''$, shifted between each other in a half period along the *a* axis. The interchange of the $[La_{1/2}O]'$ and $[La_{1/2}O]''$ layers with the [LaO] ones, along with the rock salt type cation ordering between Mg^{2+} and Ta^{5+}/W^{6+}, results in the $2a_p \times 8a_p \times 2a_p$ type superstructure. At high temperature ($T > 1400$ K) a disordered, in respect to the A-site vacancies distribution, structure is realized.

On the basis of the A-site vacancy ordering, a new homologous series, $A_{3n}B'_{2n}B''_{2n}O_{12n}$, is proposed. The members of the series have different numbers of pairs of the $[La_{1/2}O]'$ and $[La_{1/2}O]''$ layers in the unit cell (n) and are characterized by the *Ibam* space group and the $2a_p \times 4na_p \times 2a_p$ unit cell. $La_6Mg_4Ta_2W_2O_{24}$ and $La_4Mg_3W_3O_{18}$ are representatives of $n = 2$ and 1, respectively. The strategy to stabilize the members of higher n values is to decrease both the charge difference between B′ and B″ cations and the concentration of the vacancies. At the same time, the layer character of the structure and the rock salt type ionic ordering should be retained.

Acknowledgment. The authors wish to thank the Foundation for Science and Technology (FCT, Portugal) for the financial support through Grant SFRH/BPD/12669/2003.

Supporting Information Available: Bond distances, angles, and valence sums for $La_6Mg_4Ta_2W_2O_{24}$ (PDF). This material is available free of charge via the Internet at http://pubs.acs.org.

CM060916Q